

Article

2-(Arylimino)benzylidene-8-arylimino-5,6,7-trihydroquinoline Cobalt(II) Dichloride Polymerization Catalysts for Polyethylenes with Narrow Polydispersity

Zheng Zuo ¹, Qiuyue Zhang ^{1,2} , Mingyang Han ^{1,2}, Ming Liu ^{1,2} , Yang Sun ¹, Yanping Ma ¹  and Wen-Hua Sun ^{1,2,*} 

¹ Key Laboratory of Engineering Plastics and Beijing National Laboratory for Molecular Sciences, Institute of Chemistry Chinese Academy of Sciences, Beijing 100190, China

² CAS Research/Education Center for Excellence in Molecular Sciences and International School, University of Chinese Academy of Sciences, Beijing 100049, China

* Correspondence: whsun@iccas.ac.cn; Tel.: +86-10-6255-7955

Abstract: A series of 2-(arylimino)benzylidene-8-arylimino-5,6,7-trihydroquinoline cobalt(II) chlorides (**Co1–Co6**) containing a fused ring and a more inert phenyl group as the substituent at the imino-C atom has been synthesized using a one-pot synthesis method and fully characterized by FT-IR and elemental analysis. The molecular structures of **Co2** and **Co5** have been confirmed by X-ray diffraction as having a distorted square pyramidal geometry around a cobalt core with a tridentate *N,N,N*-chelating ligand and two chlorides. On activation with either methylaluminoxane (MAO) or modified methylaluminoxane (MMAO), **Co1–Co6** exhibited high activities for ethylene polymerization. The least sterically hindered **Co2** showed a maximum activity of 16.51×10^6 g (PE) mol⁻¹ (Co) h⁻¹ at a moderate temperature 50 °C. Additionally, *ortho*-fluoride **Co6** was able to maintain a high activity not only at 70 °C but also after 60 min at 50 °C, highlighting its excellent thermal-stability and long catalytic lifetime. The resultant polyethylene showed clearly narrower molecular weight distribution (*PDI*: 1.3–3.1) than those produced by structurally related cobalt counterparts, indicating the positive influence of benzhydryl substitution on the catalysis. Moreover, the molecular weight (1.7–386.6 kg mol⁻¹) of vinyl- or *n*-propyl-terminated polyethylene can be finely regulated by controlling polymerization parameters.

Keywords: homogeneous catalysis; transition metal complex; cobalt; ethylene polymerization



Citation: Zuo, Z.; Zhang, Q.; Han, M.; Liu, M.; Sun, Y.; Ma, Y.; Sun, W.-H. 2-(Arylimino)benzylidene-8-arylimino-5,6,7-trihydroquinoline Cobalt(II) Dichloride Polymerization Catalysts for Polyethylenes with Narrow Polydispersity. *Catalysts* **2022**, *12*, 1119. <https://doi.org/10.3390/catal12101119>

Academic Editors: Victorio Cadierno and Raffaella Mancuso

Received: 27 August 2022

Accepted: 22 September 2022

Published: 27 September 2022

Publisher's Note: MDPI stays neutral with regard to jurisdictional claims in published maps and institutional affiliations.

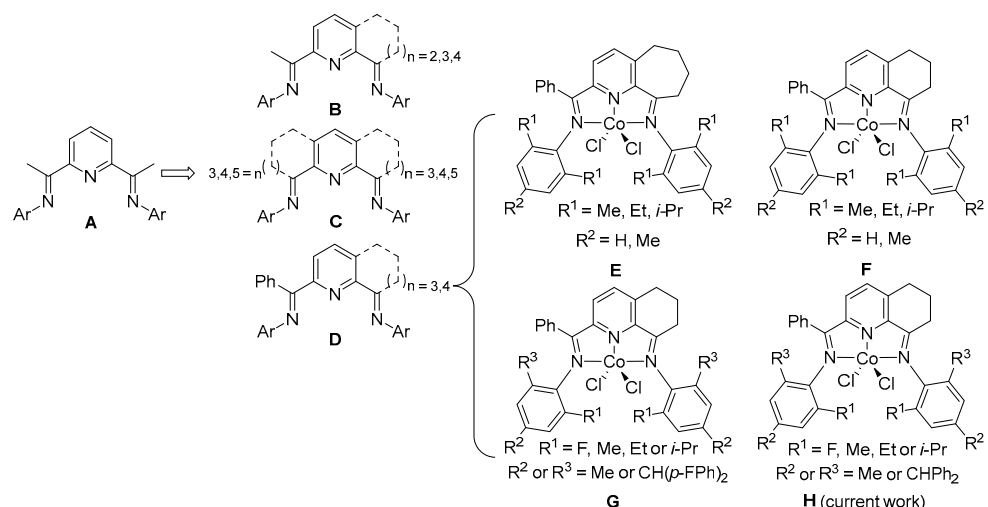


Copyright: © 2022 by the authors. Licensee MDPI, Basel, Switzerland. This article is an open access article distributed under the terms and conditions of the Creative Commons Attribution (CC BY) license (<https://creativecommons.org/licenses/by/4.0/>).

1. Introduction

In the past two decades, bis(imino)pyridyl metal (Fe or Co) precatalysts [1–26] (A, Scheme 1) have achieved great progress in ethylene polymerization and oligomerization, and therefore showed high industrial research value. However, the bis(imino)pyridine systems seemed to deactivate easily at high reaction temperatures and this observation may be attributed to the following two reasons. Firstly, these catalysts can be potentially deactivated via alkylation reactions with the alkylaluminium co-catalyst [27,28]. Secondly, the imino C-methyl groups can undergo deprotonation reactions [29,30]. In order to handle these questions, a large number of research studies [31–38] have been conducted on the structural modifications of ligands deriving from the bis(imino)pyridine framework A (Scheme 1), which mainly include the introduction of fused six, seven-membered rings and an imino C-phenyl group. Typically, iron, or cobalt complexes based on carbocyclic-fused bis(imino)pyridine ligand B, C and D (Scheme 1), were subsequently proposed. The 2,6-bis(cyclohexyl)-fused and 2,6-bis(cycloheptyl)-fused complexes B (Scheme 1) exhibited much higher activities (10.9×10^6 g (PE) mol⁻¹ (Co) h⁻¹ for **B_{hexyl}** [33]; 8.5×10^6 g (PE) mol⁻¹ (Co) h⁻¹ for **B_{heptyl}** [34] vs. 4.1×10^6 g (PE) mol⁻¹ (Co) h⁻¹ for A [1]) and better thermal stability [10.4×10^6 g (PE) mol⁻¹ (Co) h⁻¹ (70 °C) for **B_{hexyl}** [33]; 7.1×10^6 g (PE) mol⁻¹ (Co) h⁻¹ (70 °C) for **B_{heptyl}** [34] vs.

2.7×10^6 g (PE) mol⁻¹ (Co) h⁻¹ (60 °C) for **A** [1] than the prototypical 2,6-bis(imino)pyridyl cobalt complexes **A** (Scheme 1). However, the 2,6-bis(cyclopentyl)-fused **B** (Scheme 1) showed much lower catalytic activities [35] due to the inefficient imine-N coordination to the metal. In contrast, the doubly cycloheptyl-fused cobalt complexes, symmetrical **C**,_{7,7} (Scheme 1) [39] and unsymmetrical **C**,_{6,7} (Scheme 1) [40], with efficient imine-N coordination to the cobalt center showed obviously high activities and good thermal stability. Meanwhile, linear polyethylene waxes with narrow dispersity and vinyl chain ends highlight satisfying features of the polymers owing to their various applications such as lubricants and colorants for plastics processes [41]. In order to improve the rotational flexibility of the external N_{imino}-aryl group and protect the imino C-methyl groups [36–38], one type of ligand backbone **D** (Scheme 1) incorporating a fused six or seven-membered ring and an imino C-phenyl group was designed and proved to be a good candidate. For example, **E** (Scheme 1) [36] showed high activities (8.7×10^6 g PE mol⁻¹ (Co) h⁻¹) toward ethylene polymerization and exhibited good thermal stability (1.9×10^6 g PE mol⁻¹ (Co) h⁻¹, 80 °C) as well as long lifetime. When decreasing the alkyl ring size of singly fused cobalt derivatives, the significant improvement of catalytic performance has been observed. To be specific, the singly cyclohexyl-fused **F** (Scheme 1) [37] has been shown to achieve higher catalytic activity (16.2×10^6 g PE mol⁻¹ (Co) h⁻¹) with desirable thermal stability and lifetime than singly cycloheptyl-fused **E** counterpart (Scheme 1).



Scheme 1. 2,6-Bis(arylimino)pyridine-metal chloride **A** and its fused counterparts **B–H**.

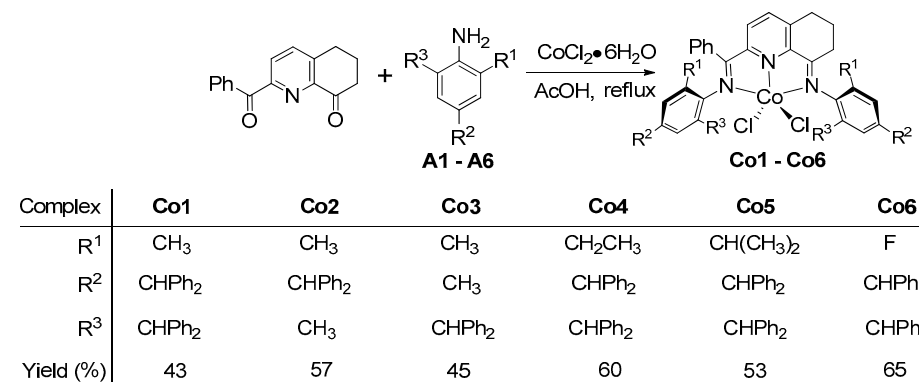
To explore the structural scope of ligand backbone based on **F** (Scheme 1), a large number of studies have involved varying the substitution pattern of the N-aryl groups. The introduction of simple alkyl groups (e.g., Me, Et, *i*-Pr) or more sterically bulky groups (e.g., benzhydryl and 4,4'-difluorobenzhydryl) into N-aryl groups, have been conducted and investigated adequately. Significantly, 4,4'-difluorobenzhydryl-substituted **G** [38] (Scheme 1) displayed high activities (27.1×10^6 g (PE) mol⁻¹ (Co) h⁻¹), good thermal stability (2.6×10^6 g (PE) mol⁻¹ (Co) h⁻¹, 70 °C) and delivered highly linear polyethylene with low molecular weight (0.69 to 31.51 kg mol⁻¹) while broad polymer dispersity (PDI up to 17.5). According to the literature [42–44], the molecular weight distributions of the polymers produced by complexes with benzhydryl tended to be narrower than those of the polymers produced by their counterparts with 4,4'-difluorobenzhydryl. The reason for this may be that the electron withdrawing capacity of the para-fluoride may decrease the electron density of the metal center and thereby decrease the chain termination energy barrier of the reaction. Consequently, the polymerization reactions would easily be affected by environmental variables, leading to the wider molecular weight distribution of the resulting polymers. Based on this consideration, benzhydryl groups were introduced to replace 4,4'-difluorobenzhydryl for the sake of obtaining polyethy-

lene with a narrower molecular weight distribution. Additionally, in order to further investigate the effect of bulky substituent type on the molecular weight distribution of resultant polyethylene and compare the catalytic behaviors between **G** (Scheme 1) and their counterparts, a series of 2-(arylimino)benzylidene-8-arylimino-5,6,7-trihydroquinoline cobalt(II) chlorides (**H**, Scheme 1), [2-(ArN=CPh)-8-(NAr)-C₉H₈N]CoCl₂ (Ar = 2-Me-4,6-((C₆H₅)₂CH)₂C₆H₂ **Co1**, 2,6-Me₂-4-((C₆H₅)₂CH)C₆H₂ **Co2**, 2,4-Me₂-6-((C₆H₅)₂CH)C₆H₂ **Co3**, 2-Et-4,6-((C₆H₅)₂CH)₂C₆H₂ **Co4**, 2-i-Pr-4,6-((C₆H₅)₂CH)₂C₆H₂ **Co5**, 2-F-4,6-((C₆H₅)₂CH)₂C₆H₂ **Co6**) was synthesized and a full catalytic evaluation (catalytic activity and polymer properties) for ethylene polymerization was conducted. Furthermore, the intrinsic properties (e.g., molecular weight, molecular weight distributions, melting temperatures, microstructure) of the polyethylene were fully characterized and discussed in detail.

2. Results and Discussion

2.1. Preparation and Characterization of **Co1–Co6**

Due to the large steric hindrance of benzoyl group, it is difficult to isolate the bis(arylimine) ligands. Therefore, in this work, cobalt complexes were synthesized by the metal template method. Specifically, 2-(arylimino)benzylidene-8-arylimino-5,6,7-trihydroquinoline cobalt(II) dichloride complexes, [2-(ArN=CPh)-8-(NAr)-C₉H₈N]CoCl₂ (Ar = 2-Me-4,6-(CH(C₆H₅)₂)₂C₆H₂ (**Co1**), 4-(CH(C₆H₅)₂)-2,6-Me₂C₆H₂ (**Co2**), 2,4-Me₂-6-(CH(C₆H₅)₂)C₆H₂ (**Co3**), 2-Et-4,6-(CH(C₆H₅)₂)₂C₆H₂ (**Co4**), 2-i-Pr-4,6-(CH(C₆H₅)₂)₂C₆H₂ (**Co5**), 2-F-4,6-(CH(C₆H₅)₂)₂C₆H₂ (**Co6**)), can be prepared in high yield (43–65%) by the one-pot reaction of 1 equiv. 2-benzoyl-5,6,7-trihydroquinolin-8-one, 4 equiv. aniline (**A1–A6**) and 0.8 equiv. cobalt(II) chloride in refluxing acetic acid (Scheme 2).



Scheme 2. One-flask assembly of cobalt complexes **Co1–Co6**.

All the cobalt complexes have been fully characterized by FT-IR and elemental analysis. In their FT-IR spectra, all cobalt complexes (**Co1–Co6**) displayed a clear imine (C = N) absorption band (1600 cm^{−1}) indicating the effective coordination state between the cobalt center with the N_{imine} atom. Meanwhile, the elemental analysis data confirmed the molecular formulae as LCoCl₂ for all cobalt complexes. In addition, the molecular structures of **Co2** and **Co5** were confirmed by the single-crystal X-ray diffraction. Their molecular structures are shown in Figures 1 and 2, respectively, and the selected bond lengths and angles are listed in Table 1. In both molecular structures, the distorted square pyramidal coordination geometry can be observed in which one chloride ligand (Cl1) occupies the apical position while three nitrogen donors and the remaining chloride (Cl2) form the square basal plane. This distortion makes the cobalt center of **Co2** and **Co5** sit above the basal plane at a distance of 0.372 and 0.342 Å, respectively. Moreover, the bond lengths of Co–N_{pyridyl} (**Co1**–N2: 2.051(8) Å **Co2** and 2.051(2) Å **Co5**) are shorter than the exterior Co–N_{imine} bond lengths (**Co1**–N1: 2.295(7) Å **Co2** and 2.310(3) Å **Co5**; **Co1**–N3: 2.258(8) Å **Co2** and 2.214(2) Å **Co5**), indicating the existence of more effective coordination between Co and N_{pyridyl} atoms; similar features have been observed in structurally related cobalt analogues [33]. Due to the steric hindrance in the ligand skeleton, there are N1–C7–C8–

N2 and N3–C16–C12–N2 torsion angles (9.9° , 2.8° for **Co2**; 17.5° , 8.6° for **Co5**) within the *N,N,N*-ligand consistent with the fact that *N*-aryl groups tend to deviate from the coordination planarity.

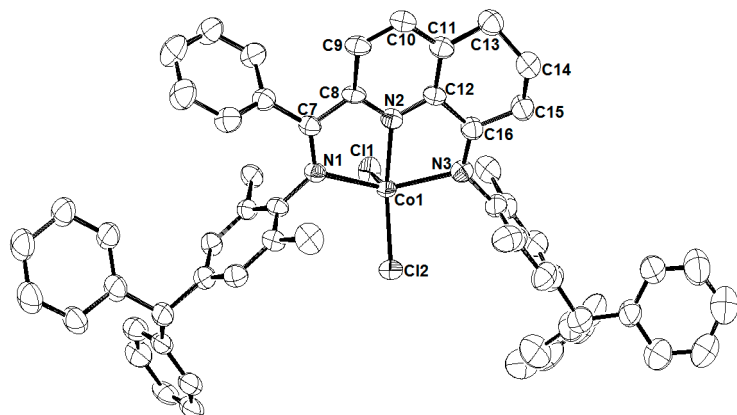


Figure 1. ORTEP representation of **Co2** with the thermal ellipsoids shown at the 30% probability level. Hydrogen atoms are omitted for clarity.

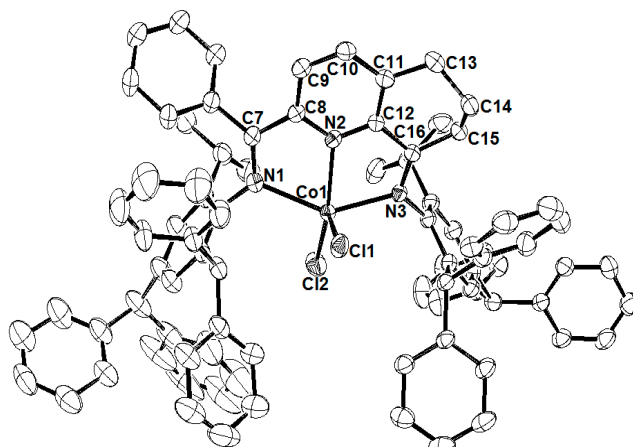


Figure 2. ORTEP representation of **Co5** with the thermal ellipsoids shown at the 30% probability level. One molecule of **Co5** and hydrogen atoms are omitted for clarity.

2.2. Catalytic Evaluation of **Co1–Co6** for Ethylene Polymerization

Normally, the alkyl aluminoxane reagents, namely methylaluminoxane (MAO) and modified methylaluminoxane (MMAO), as the best activators were used to activate cobalt pre-catalysts for ethylene polymerization [45,46]. Therefore, MAO and MMAO were used for the detailed studies of ethylene polymerization, separately. In both studies, the optimal parameters such as polymerization temperature, Al:Co molar ratio, polymerization time and ethylene pressure were screened using *ortho*-fluoride **Co6** as the test pre-catalyst. Then, the remaining five cobalt complexes (**Co1–Co5**) were evaluated based on the optimum polymerization condition. Differential scanning calorimetry (DSC) and gel permeation chromatography (GPC) were used to characterize all polymers to understand their nature. In addition, high temperature ^1H NMR, ^{13}C NMR, DEPT-135 ^{13}C NMR and FT-IR spectroscopy were used to analyze the microstructural properties of the selected polyethylene.

2.2.1. Optimization of the Polymerization Conditions Using **Co6**/MAO

The run temperature of **Co6**/MAO catalytic system was firstly screened from $30\text{ }^\circ\text{C}$ to $70\text{ }^\circ\text{C}$ when the Al:Co molar ratio and run time were set as 2000:1 and 30 min, respectively (entries 1–5, Table 2).

Table 1. Selected bond lengths (Å) and angles (°) for **Co2** and **Co5**.

	Co2	Co5
Bond lengths (Å)		
Co(1)–Cl(2)	2.239(3)	2.1984(10)
Co(1)–Cl(1)	2.256(3)	2.2914(10)
Co(1)–N(2)	2.051(8)	2.051(2)
Co(1)–N(1)	2.295(7)	2.310(3)
Co(1)–N(3)	2.258(8)	2.214(2)
N(2)–C(12)	1.368(12)	1.343(4)
N(2)–C(8)	1.349(11)	1.335(4)
N(1)–C(7)	1.286(11)	1.288(4)
N(3)–C(16)	1.242(12)	1.285(4)
Bond angles (°)		
Cl(1)–Co(1)–Cl(2)	117.10(13)	117.32(4)
N(1)–Co(1)–N(3)	145.4(3)	146.07(9)
N(1)–Co(1)–Cl(1)	99.1(2)	99.37(7)
N(1)–Co(1)–Cl(2)	97.35(2)	99.04(7)
N(2)–Co(1)–Cl(1)	103.6(2)	92.64(8)
N(2)–Co(1)–Cl(2)	139.3(2)	150.02(8)
N(2)–Co(1)–N(3)	74.7(3)	75.42(9)
N(1)–Co(1)–N(2)	73.5(3)	73.10(9)
N(3)–Co(1)–Cl(1)	101.2(2)	94.35(7)
N(3)–Co(1)–Cl(2)	97.9(2)	101.91(7)

Table 2. Catalytic evaluation using **Co6**/MAO as the test system ^a.

Entry	T (°C)	Al:Co	t (min)	Mass of PE (g)	Activity ^b	T _m ^c (°C)	M _w ^d	M _w /M _n ^d	R _i ^e	R _t ^f
1	30	2000	30	2.3	2.3	123.9	1.5	1.5	164.0	4600.0
2	40	2000	30	3.7	3.7	123.6	1.6	1.8	263.8	8325.0
3	50	2000	30	6.9	6.9	122.6	1.7	1.5	492.0	12,176.5
4	60	2000	30	6.1	6.1	120.2	2.4	1.7	434.9	8641.7
5	70	2000	30	2.9	2.9	122.8	2.2	1.5	206.8	3954.5
6	50	1750	30	6.3	6.3	121.9	1.5	2.1	449.2	17,640.0
7	50	2250	30	6.5	6.5	122.1	1.6	1.5	463.5	12,187.5
8	50	2500	30	6.5	6.5	121.5	1.6	1.5	463.5	12,187.5
9	50	2750	30	6.6	6.6	121.8	1.6	1.6	470.6	13,200.0
10	50	3000	30	5.6	5.6	121.8	1.5	2.0	399.3	14,933.3
11	50	4000	30	5.5	5.5	122.5	1.3	1.4	392.2	11,846.2
12	50	2000	5	3.9	23.1	118.9	1.3	1.4	1668.4	50,400.0
13	50	2000	15	4.8	7.7	120.5	1.5	1.5	684.5	19,200.0
14	50	2000	45	6.3	4.2	121.1	1.7	1.6	299.5	7905.9
15	50	2000	60	8.2	4.1	123.2	1.9	1.7	292.3	7336.8
16 ^g	50	2000	30	2.1	2.1	122.4	1.1	1.3	149.7	4963.6
17 ^h	50	2000	30	-	-	-	-	-	-	-

^a General conditions: 2.0 μmol **Co6**, 100 mL toluene, P_{C2H4} = 10 atm. ^b 10⁶ g (PE)·mol⁻¹ (Co)·h⁻¹. ^c Determined by DSC. ^d M_w (kg mol⁻¹) and M_w/M_n were determined by GPC. ^e Rate of monomer insertion, in units of mmol/h. ^f Rate of chain termination, in units of μmol/h. ^g P_{C2H4} = 5 atm. ^h P_{C2H4} = 1 atm.

50 °C was found as the most suitable temperature affording highest activity of 6.9×10^6 g (PE) mol⁻¹ (Co) h⁻¹ (entry 3, Table 2). When the temperature was raised to 70 °C, the catalytic activity of **Co6**/MAO sharply decreased to 2.9×10^6 g (PE) mol⁻¹ (Co) h⁻¹ due to partial decomposition of the active species and low solubility of ethylene in toluene at high temperature (Figure 3b). As shown in Figure 3, the GPC curves verified the increasing tendency of molecular weights from 1.5 to 2.4 kg mol⁻¹ along with the increasing temperature. The reason for this may be that the proportion of the chain propagation path increased at a higher temperature [47]. Molecular weights increased progressively from 1.7 kg mol⁻¹ at 50 °C to 2.4 kg mol⁻¹ at 60 °C (entry 3 and 4, Table 2), which can

be mainly credited to the sharply decreased chain termination rate (R_t range: 12,176.5 to 8641.7 $\mu\text{mol}/\text{h}$). Similar conclusions have been reached elsewhere [48,49]. Meanwhile, the bimodal distribution can be explained by the bimodality active center formed at a high temperature.

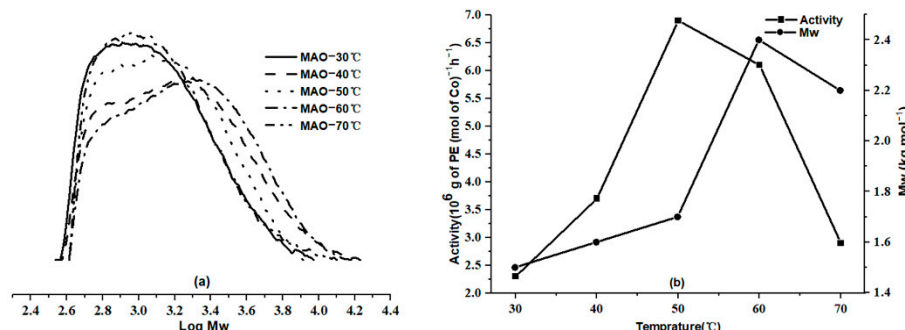


Figure 3. For Co6/MAO: (a) GPC traces of the polyethylene obtained at different run temperature; and (b) plots of catalytic activity and M_w of the resultant PE as a function of run temperature (entries 1–5, Table 2).

On varying molar ratios of Al:Co from 1750:1 to 4000:1 at 50 °C (entries 3, 6–11, Table 2), the best activity up to $6.9 \times 10^6 \text{ g(PE) mol}^{-1} (\text{Co}) \text{ h}^{-1}$ was still observed at 2000:1 (entry 3, Table 2). Further increasing Al/Co molar ratio to 3000:1, the activity slightly decreased to $5.6 \times 10^6 \text{ g(PE) mol}^{-1} (\text{Co}) \text{ h}^{-1}$. There was no significant change in activity value when the molar ratio was above 3000:1 (Figure 4b). Additionally, the molecular weights of the resultant polyethylene showed a stable trend as the molar ratio of Al:Co increased, which can plausibly be attributed to β-H elimination as the main chain termination pathway rather than chain transfer to aluminum. Generally, all the polyethylene obtained at different Al:Co molar ratios possessed low-molecular weights ($M_w = 1.3\text{--}1.7 \text{ kg mol}^{-1}$) and narrow molecular weight distributions ($M_w/M_n = 1.5\text{--}2.1$).

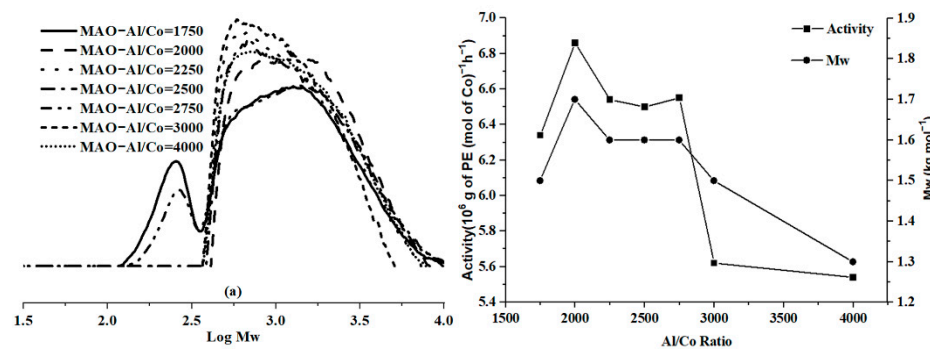


Figure 4. For Co6/MAO: (a) GPC traces of the polymers obtained at different Al:Co molar ratios; and (b) plots of catalytic activity and M_w of the resultant PE as a function of Al:Co molar ratio (entries 3, 6–11, Table 2).

Applying the optimized reaction parameters (Al:Co molar ratio = 2000:1 and temperature = 50 °C) on ethylene polymerization, the lifetime (5–60 min) of Co6/MAO catalytic system was extensively investigated (entries 3 and 12–15, Table 2). The highest activity ($23.1 \times 10^6 \text{ g(PE) mol}^{-1} (\text{Co}) \text{ h}^{-1}$) was observed within 5 min (entry 12, Table 2), indicating that there was no induction period in the whole polymerization process, which was similar to previous work [50]. On prolonging the polymerization time to 60 min, catalytic activities were gradually decreased to a minimum value of $4.1 \times 10^6 \text{ g(PE) mol}^{-1} (\text{Co}) \text{ h}^{-1}$ (Figure 5). This finding suggests that the active species underwent a steady deactivation process over time. However, the activity observed at 60 min ($4.1 \times 10^6 \text{ g(PE) mol}^{-1} (\text{Co}) \text{ h}^{-1}$) was comparable to that observed at 45 min ($4.2 \times 10^6 \text{ g(PE) mol}^{-1} (\text{Co}) \text{ h}^{-1}$) implying a con-

siderable lifetime of this class of catalyst. In terms of the molecular weight of the resultant polyethylene, their value increased from 1.3 kg mol^{-1} to 1.9 kg mol^{-1} as the run time was prolonged from 5 min to 60 min, which indicates the catalyst can maintain continuous chain propagation over time.

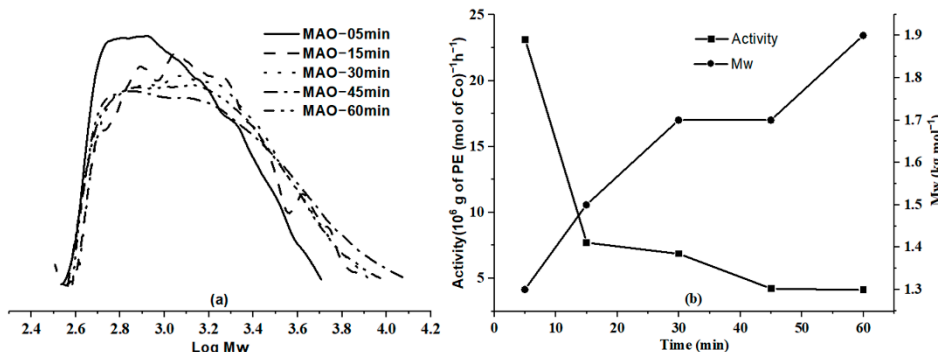


Figure 5. For **Co6**/MAO: (a) GPC traces of the polyethylene obtained at different reaction times; and (b) plots of catalytic activity and M_w of the resultant PE as a function of reaction time (entries 3, 12–15, Table 2).

Subsequently, ethylene polymerization under low pressure (1 or 5 atm) was further explored. With the decrease of ethylene pressure, the catalytic activity decreased significantly to $2.1 \times 10^6 \text{ g (PE) mol}^{-1} (\text{Co}) \text{ h}^{-1}$ at 5 atm while only trace polymer was obtained at 1 atm (entries 16, 17, Table 2). Two possible reasons could be used to explain this observation. Firstly, the lower the ethylene pressure, the less easy the coordination and insertion reaction of ethylene. Secondly, low ethylene pressure will reduce the solubility of ethylene monomer in toluene. For the same reason, the molecular weight of the polymer decreased from 1.7 kg mol^{-1} (10 atm, entries 3 in Table 2) to 1.1 kg mol^{-1} (5 atm, entries 16 in Table 2).

2.2.2. Catalytic Evaluation of **Co1–Co6** Using MAO as Co-Catalyst under the Optimal Conditions

Under the optimum conditions [Al:Co molar ratio = 2000:1, polymerization temperature = 50°C and run time = 30 min, $P_{\text{C}_2\text{H}_4} = 10 \text{ atm}$] established for **Co6**/MAO, the remaining cobalt complexes **Co1–Co5** have been employed to study the effect of ligand structure on catalytic activity and polymer properties; the polymerization results are collected in Table 3.

Table 3. Ethylene Polymerization using **Co1–Co6** with MAO as the co-catalyst ^a.

Entry	Precat.	Mass of PE (g)	Activity ^b	T _m ^c ($^\circ\text{C}$)	M _w ^d	M _w /M _n ^d	R _i ^e	R _t ^f
1	Co1	5.1	5.1	133.9	68.2	2.7	363.6	403.8
2	Co2	16.5	16.5	123.9	3.3	1.4	1176.5	14,000.0
3	Co3	5.0	5.0	132.5	55.4	1.4	356.5	252.7
4	Co4	3.9	3.9	132.4	62.8	2.8	278.1	347.8
5	Co5	3.8	3.8	134.7	198.7	1.7	270.9	65.0
6	Co6	6.9	6.9	122.6	1.7	1.5	492.0	12,176.5

^a General conditions: 2.0 μmol cobalt precatalyst, 100 mL toluene, $P_{\text{C}_2\text{H}_4} = 10 \text{ atm}$, 30 min, 50°C , Al:Co molar ratio of 2000:1. ^b $10^6 \text{ g (PE) mol}^{-1} (\text{Co}) \text{ h}^{-1}$. ^c Determined by DSC. ^d M_w (kg mol^{-1}) and M_w/M_n were determined by GPC. ^e Rate of monomer insertion, in units of mmol/h. ^f Rate of chain termination, in units of $\mu\text{mol}/\text{h}$.

All cobalt catalysts displayed high activities in the range of $3.8\text{--}16.5 \times 10^6 \text{ g (PE) mol}^{-1} (\text{Co}) \text{ h}^{-1}$, and their activities were found to decrease as the following order: **Co2** [2,6-Me₂-4-(CH(C₆H₅)₂)] >> **Co6** [2-F-4,6-(CH(C₆H₅)₂)₂] > **Co1** [2-Me-4,6-(CH(C₆H₅)₂)₂] > **Co3** [2,4-Me₂-6-(CH(C₆H₅)₂)] > **Co4** [2-Et-4,6-(CH(C₆H₅)₂)₂] ~ **Co5** [2-i-Pr-4,6-(CH(C₆H₅)₂)₂]. Several points are outlined as follows according to the analysis of the catalytic activity trend of the complexes. The **Co2** containing two methyl groups at the *ortho*-position of the

N-aryl group showed the highest activity up to $16.5 \times 10^6 \text{ g (PE)·mol}^{-1} (\text{Co})\cdot\text{h}^{-1}$ (entry 2, Table 3) among this set. This may be due to the low resistance effect of *ortho*-substituents, which made the monomer easier to approach the metal center. Moreover, **Co6** containing the strongly electron-withdrawing *fluoro*-substituents at the *ortho*-position of the *N*-aryl group had the second highest activity of $6.9 \times 10^6 \text{ g (PE)·mol}^{-1} (\text{Co})\cdot\text{h}^{-1}$ (entry 6, Table 3). This finding can be attributed to the fact that the electron withdrawing group reduced the electron density of the metal center leading to easier chain growth step [51]. In contrast, those cobalt complexes containing electron-donating groups (Me (**Co1** and **Co3**), Et (**Co4**), *i*-Pr (**Co5**)) were less active with catalytic activity ranged from 3.8 to $5.1 \times 10^6 \text{ g (PE)·mol}^{-1} (\text{Co})\cdot\text{h}^{-1}$ (entry 1, 3–5, Table 3).

However, with **Co3**, the type of substituent at the *N*-aryl para-position has little effect on the catalytic activity, which can be exemplified by comparing the catalytic activity values of **Co1** (*para*-R² = CHPh₂, $5.1 \times 10^6 \text{ g (PE)·mol}^{-1} (\text{Co})\cdot\text{h}^{-1}$) and **Co3** (*para*-R² = Me, $5.0 \times 10^6 \text{ g (PE)·mol}^{-1} (\text{Co})\cdot\text{h}^{-1}$). In terms of polymer molecular weight, the space volume of the *N*-aryl *ortho*-substituents played an essential role in controlling the molecular weights of the resultant polyethylene. The molecular weight of the polymer obtained using **Co5** (up to $198.7 \text{ kg mol}^{-1}$) was over 50 times higher than that of the polymer obtained using **Co2** (3.3 kg mol^{-1}) and more than 100 times higher than that of the polymer obtained using **Co6** (1.7 kg mol^{-1}), which may be because the spatial volume of *ortho*-substituents in *N*-aryl group can provide greater steric protection for the active center to prevent chain termination reaction (entry 5, Table 3). **Co2** and **Co6** produce polyethylene with low molecular weight (3.3 (**Co2**), 1.7 (**Co6**)), which can be mainly credited to the large chain termination rate (R_t : 14000.0 (**Co2**), 12176.5 (**Co6**)). Similar conclusions have been reached elsewhere [48,49]. It is obvious that the order of catalytic activity values was opposite to that of polymer molecular weight values (Figure 6). Most importantly, current catalytic system could afford polyethylene with narrower molecular weight distribution (M_w/M_n range: 1.4–2.8) than its counterparts substituted by 4,4'-difluorobenzhydryl (**G**, Scheme 1) [38].

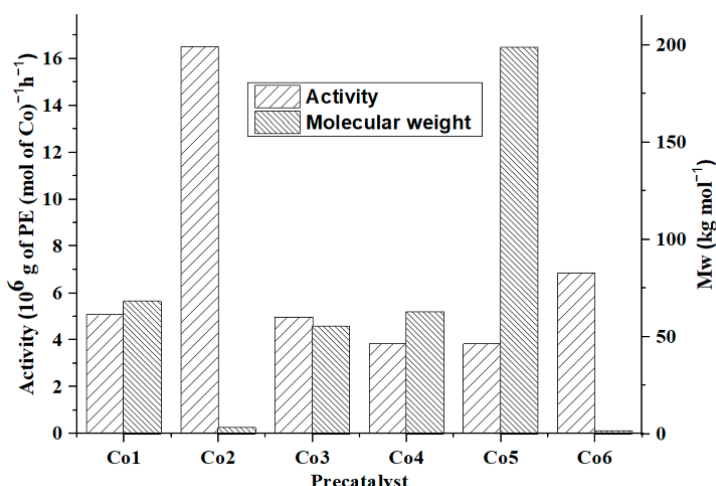


Figure 6. Catalytic activities and molecular weight of the polyethylene produced using **Co1**–**Co6**; MAO as co-catalyst in each case (entries 1–6, Table 3).

2.2.3. Optimization of the Polymerization Conditions Using **Co6**/MMAO

In the presence of MMAO, the pre-catalyst **Co6** was again employed to optimize the reaction conditions of ethylene polymerization; the results were tabulated in Table 4.

Table 4. Catalytic evaluation using **Co6**/MMAO as the test system ^a.

Entry	T (°C)	Al:Co	t (min)	Mass of PE (g)	Activity ^b	T _m ^c (°C)	M _w ^d	M _w /M _n ^d	R _i ^e	R _t ^f
1	30	2000	30	1.9	1.9	123.1	3.7	1.1	135.5	1129.7
2	40	2000	30	2.4	2.4	121.7	2.4	1.3	171.1	2600.0
3	50	2000	30	2.2	2.2	121.5	2.1	1.3	156.9	2723.8
4	60	2000	30	1.5	1.5	120.6	5.0	1.7	107.0	1020.0
5	40	2250	30	5.4	5.4	122.0	2.7	1.3	385.0	5200.0
6	40	2500	30	2.5	2.5	121.9	2.4	1.3	178.3	2708.3
7	40	2750	30	1.5	1.5	122.9	2.6	1.3	107.0	1500.0
8	40	3000	30	1.1	1.1	122.4	2.8	1.4	78.4	1100.0
9	40	2250	5	3.3	19.8	119.9	1.8	1.3	1411.8	28,600.0
10	40	2250	15	4.2	8.4	121.6	2.6	1.3	598.9	8400.0
11	40	2250	45	7.9	5.2	121.8	2.8	1.3	375.5	4890.5
12	40	2250	60	10.2	5.1	122.2	6.1	2.1	363.6	3511.5
13 ^g	40	2250	30	1.2	1.2	121.5	1.1	1.3	85.6	2836.4
14 ^h	40	2250	30	-	-	-	-	-	-	-

^a General conditions: 2.0 μmol **Co6**, 100 mL toluene, P_{C2H4} = 10 atm. ^b 10⁶ g (PE)·mol⁻¹ (Co)·h⁻¹. ^c Determined by DSC. ^d M_w (kg mol⁻¹) and M_w/M_n were determined by GPC. ^e Rate of monomer insertion, in units of mmol/h. ^f Rate of chain termination, in units of μmol/h. ^g P_{C2H4} = 5 atm. ^h P_{C2H4} = 1 atm.

With the Al:Co molar ratio fixed at 2000:1 and run time kept to 30 min, the reaction temperature was screened from 30 to 60 °C (entries 1–4, Table 4). The optimum temperature was found as 40 °C and the best activity was up to 2.4 × 10⁶ g (PE) mol⁻¹ (Co) h⁻¹ (entry 2, Table 4). At higher reaction temperature, the activity gradually decreased to 1.5 × 10⁶ g (PE) mol⁻¹ (Co) h⁻¹ (Figure S1) and this behavior may result from the partial inactivation of active species (Figure S1) or the lower solubility of ethylene in toluene under high temperature. Regarding the obtained polyethylene, the molecular weights gradually declined to 2.1 kg mol⁻¹ as the temperature increased to 50 °C, which may be due to faster chain termination at a higher temperature [47]. As we can seen from Table 4, the molecular weights again showed a decreased trend from 30 °C to 50 °C (entry 1–3, Table 4) due to the increased chain termination rate (R_t range: 1129.7 to 2723.8 μmol/h). Similar conclusions have been reached elsewhere [48,49]. In comparison with the results of the **Co6**/MAO system, the **Co6**/MMAO system showed slightly lower activity, but the resultant polyethylene possessed larger molecular weight and similarly narrow polydispersity. This may be due to the different effects of co-catalyst type on the activation mode and the type of active center in the polymerization process.

On varying the Al:Co ratios from 2000:1 to 3000:1 (entries 2, 5–8, Table 4) with the temperature fixed at 40 °C, the optimal Al:Co molar ratio was found as 2250:1 with the optimal activity of 5.4 × 10⁶ g (PE) mol⁻¹ (Co) h⁻¹ (entry 5, Table 4). When the molar ratio was 2500:1 or higher, the activity showed a modest decrease (entries 6–8, Table 4). There was no significant change in molecular weights of polyethylene as the Al:Co molar ratio increased (Figure S2). Additionally, the resultant polyethylene obtained at different Al/Co molar ratios had unimodal and narrow molecular weight distribution (M_w/M_n range: 1.3–1.4), suggesting the existence of single-site active species at 50 °C.

In order to explore the lifetime of active species in the **Co6**/MMAO system, the polymerization time was varied between 5 and 60 min with Al:Co molar ratio and polymerization temperature fixed at 2250:1 and 40 °C, respectively (entries 5 and 9–12, Table 4). The polymerization results showed that the maximum catalytic activity was 19.8 × 10⁶ g (PE) mol⁻¹ (Co) h⁻¹ after 5 min (entry 9, Table 4), while the activity decreased steadily with the extension of reaction time (Figure S3). Similar with the long-time polymerization of **Co**/MAO system, this high polymerization activity present in the early stage of polymerization supported by **Co**/MMAO system highlights the short induction period of this system. Nevertheless, although the catalyst partially decayed, it still maintained high activity within 60 min, highlighting the appreciable lifetime of this catalytic system. Despite

some evidence of deactivation, the molecular weight of the polymer can still increase from 1.8 kg mol^{-1} after 5 min to 6.1 kg mol^{-1} after 60 min, which indicates the catalyst was able to maintain continuous chain growth.

In addition to the above screening of polymerization conditions, a study as to the effects of ethylene pressure was also conducted using **Co6**/MMAO at 40°C (entries 13–14, Table 4). When the pressure dropped to 5 atm, the activity value was $1.2 \times 10^6 \text{ g (PE) mol}^{-1} (\text{Co}) \text{ h}^{-1}$, which was noticeably lower than that observed at 10 atm ($5.4 \times 10^6 \text{ g (PE) mol}^{-1} (\text{Co}) \text{ h}^{-1}$) (entry 5, Table 4), while at 1 atm no polymer could be detected. Similar observations were noted with **Co6**/MAO system, which can be attributed to the effects of different pressure on coordination/insertion rate of ethylene and the solubility of the ethylene monomer in the reaction solvent. For similar reasons, it can be explained that the molecular weight of the polymer showed a downward trend as the pressure decreased (from 2.7 kg mol^{-1} at 10 atm to 1.1 kg mol^{-1} at 5 atm).

2.2.4. Catalytic Evaluation of **Co1**–**Co6** Using MMAO as Co-Catalyst under the Optimal Conditions

Under the optimum conditions (Al:Co molar ratio = 2250:1, polymerization temperature = 40°C , run time = 30 min and $P_{\text{C}_2\text{H}_4} = 10 \text{ atm}$), the other five cobalt pre-catalysts (**Co1**–**Co5**) were also investigated for the ethylene polymerization; the results are listed in Table 5.

Table 5. Ethylene Polymerization using **Co1**–**Co6** with MMAO as the co-catalyst ^a.

Entry	Precat.	Mass of PE (g)	Activity ^b	T_m ^c ($^\circ\text{C}$)	M_w ^d	M_w/M_n ^d	R_i ^e	R_t ^f
1	Co1	4.3	4.3	133.5	81.6	1.8	306.6	189.7
2	Co2	11.1	11.1	123.4	3.6	1.5	791.4	9250.0
3	Co3	4.1	4.1	134.1	138.5	3.1	292.3	183.5
4	Co4	3.7	3.7	134.4	150.2	2.9	263.8	142.9
5	Co5	3.1	3.1	134.7	386.6	2.3	221.0	36.9
6	Co6	5.4	5.4	122.0	2.7	1.3	385.0	5200.0

^a General conditions: 2.0 μmol cobalt precatalyst, 100 mL toluene, $P_{\text{C}_2\text{H}_4} = 10 \text{ atm}$, 30 min, 40°C , Al:Co molar ratio of 2250:1. ^b $10^6 \text{ g (PE) mol}^{-1} (\text{Co}) \text{ h}^{-1}$. ^c Determined by DSC. ^d M_w (kg mol^{-1}) and M_w/M_n were determined by GPC. ^e Rate of monomer insertion, in units of mmol/h. ^f Rate of chain termination, in units of $\mu\text{mol}/\text{h}$.

Generally, all the cobalt pre-catalysts showed the similar order of activities as observed for the **Co**/MAO system: **Co2** [2,6-Me₂-4-(CH(C₆H₅)₂)] >> **Co6** [2-F-4,6-(CH(C₆H₅)₂)₂] > **Co1** [2-Me-4,6-(CH(C₆H₅)₂)₂] ~ **Co3** [2,4-Me₂-6-(CH(C₆H₅)₂)] > **Co4** [2-Et-4,6-(CH(C₆H₅)₂)₂] > **Co5** [2-*i*-Pr-4,6-(CH(C₆H₅)₂)₂]. Comparing with the **Co**/MAO system, all the cobalt pre-catalysts in **Co**/MMAO set exhibited slightly lower activities but delivered polyethylene with higher molecular weights (up to $386.6 \text{ kg mol}^{-1}$, entry 5 in Table 5). Among all the pre-catalysts, the least sterically bulky **Co2** complex exhibited the highest activity of $11.1 \times 10^6 \text{ g (PE) mol}^{-1} (\text{Co}) \text{ h}^{-1}$; *ortho*-fluoro substituted **Co6** exhibited the second highest activity of $5.4 \times 10^6 \text{ g (PE) mol}^{-1} (\text{Co}) \text{ h}^{-1}$. The excellent properties of **Co6** can be explained by the electron withdrawing properties of *ortho*-fluorine atoms. For the properties of resultant polyethylene, the molecular weight of the polymer obtained using **Co5** ($386.6 \text{ kg mol}^{-1}$) was much higher than that of the polymer obtained using **Co2** (3.6 kg mol^{-1}) and **Co6** (2.7 kg mol^{-1}), which may be due to the steric bulk substitution at *ortho*-position of the N-aryl group. **Co2** and **Co6** produce polyethylene with low molecular weight (3.6 (**Co2**)), 2.7 (**Co6**)), which can be credited to the large chain termination rate (R_t : 9250.0 (**Co2**), 5200.0 (**Co6**)). Similar conclusions have been reached elsewhere [48,49]. In common with the study of **Co**/MAO system, the order between molecular weight and activity also showed an obvious opposite trend (Figure S4). In particular, the dispersities for the obtained polyethylene were narrow (M_w/M_n range: 1.3–3.1) and unimodal, indicating that the benzoyl group is conducive to regulating the single active center state of the catalytic center. Meanwhile, the high melting temperatures (T_m range: 122.0–134.7 $^\circ\text{C}$) of resultant polyethylene demonstrates the high linearity of polyethylene [52,53].

In order to compare the catalytic performance of the current catalytic system with structurally related cobalt catalysts [33,34,38,50], the key performance data relating to activity, the molecular weight and PDI of polymer obtained by **I–L** and **Co2** under their optimized conditions with MAO as co-catalyst were collected in Figure 7.

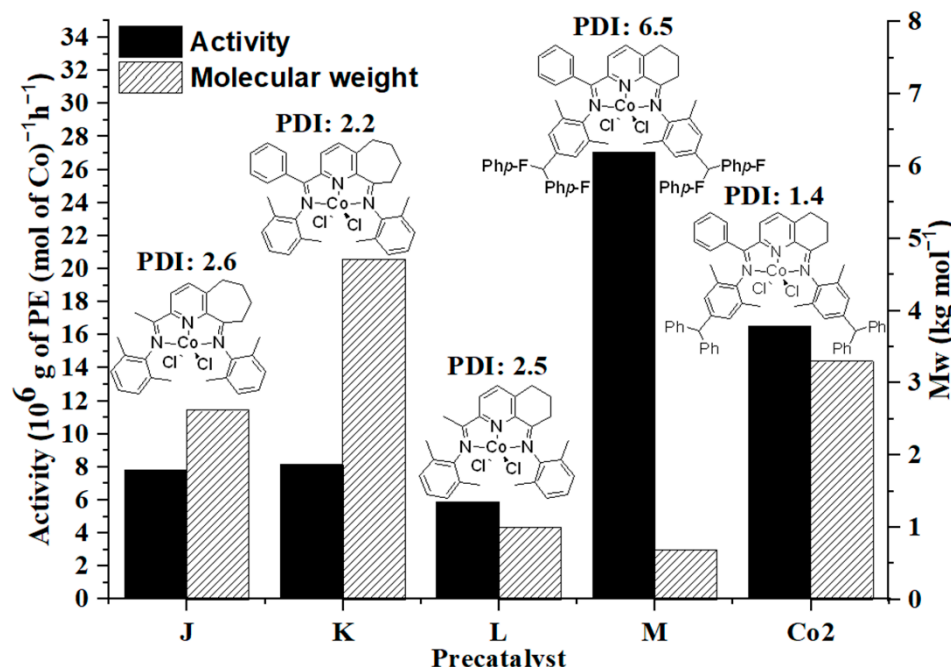


Figure 7. Comparative catalytic performance of **I–L** with **Co2** (entry 2, Table 3) under their respective optimum conditions.

The data inspection in Figure 7 mainly reveals the following several points. Firstly, the introduction of imino-C phenyl group has a positive effect on increasing the molecular weight of the obtained polyethylene. For instance, complex **I** [34] could produce polyethylene with higher molecular weight than those prepared by complex **J** [50]. This observation may be due to the protective effect of phenyl on the active center. Secondly, the increase of ring size had a favorable effect on the molecular weight of polyethylene. The molecular weight obtained with complex **I** was significantly higher than that obtained with complex **K** [33], and their activities were comparable with each other. Thirdly, the introduction of 4,4'-difluorobenzhydryl and benzhydryl groups can greatly improve catalytic activity of complex. For example, **L** [38] and **Co2** was more active than **I–K**, which can be attributed to the electron withdrawing capacity of the 4,4'-difluorobenzhydryl and benzhydryl groups being able to decrease the electron density of the metal center and thereby making chain propagation more facile. Fourthly, the molecular weight distribution of the polymer produced by cobalt complex with benzhydryl (PDI = 1.4, **Co2**) was much narrower than that of the polymer produced by its counterparts with 4,4'-difluorobenzhydryl (PDI = 6.5, **L**), indicating the positive influence of benzhydryl substitution on the single site catalytic behavior of cobalt catalysts. The reason may be that the chain termination energy barrier of the remote fluorine substituted complexes is low and the polymerization reactions may be easily affected by environmental variables, making the molecular weight distribution of the resulting polymers wider.

2.3. Microstructural Properties of Resultant Polyethylenes

To further explore the microstructural properties of these resultant polyethylene, high temperature ^1H and ^{13}C NMR spectroscopy was used to record two representative samples generated using **Co2**/MAO ($M_w = 3.3 \text{ kg/mol}$, entry 2, in Table 3) and **Co2**/MMAO ($M_w = 3.6 \text{ kg/mol}$, entry 2, in Table 5). To meet the requirements for sample solubility,

these NMR spectra were recorded at 100 °C in d_2 -tetrachloroethane. For the two samples mentioned above, their ^1H and ^{13}C NMR spectra displayed a singlet of high intensity with chemical shifts (δ H 1.34 ppm; δ C 29.07 ppm) that were characteristic of the $-(\text{CH}_2)_n-$ repeat unit in accord with strictly linear polyethylene (Figures 8 and S5). Less intense downfield peaks with chemical shifts (δ 5.90 (H_b) and δ 5.04 (H_a); δ 113.87 (C_a) and 139.03 (C_b)) can be assigned to vinyl end groups ($-\text{CH}=\text{CH}_2$). Additionally, the integral of H_g (δ 0.95) was three times larger than that of H_b (δ 5.90) in both cases in accordance with the presence of some saturated polyethylene. According to the integration results, it can be known that polymers with vinyl end groups ($-\text{CH}=\text{CH}_2$) were the main polymerization products indicating that β -H elimination was the major chain termination pathway. In order to prove the correctness of the structure revealed by NMR, we also tested the above polymers by DEPT-135 ^{13}C NMR and FT-IR spectroscopy. The DEPT-135 ^{13}C NMR spectra showed that the positive CH and CH_3 peaks and negative CH_2 peaks were present at reasonable positions in line with the proposed microstructure of the resultant polymers (Figures S6 and S7). We also recorded the FT-IR spectroscopy of polymers formed by **Co2** (MAO: Al/Co = 2000:1 and MMAO: Al/Co = 2250:1) (entry 2, Table 3; entry 2, Table 5), **Co6** (MAO: Al/Co = 2000:1, 2500:1 and MMAO: Al/Co = 2250:1, 2750:1) (entry 3, Table 2; entry 8, Table 2; entry 5, Table 4; entry 7, Table 4). As shown in Figure S8 and S9, these spectra reveal strong peaks at 710–740 cm^{-1} (CH_2 rocking vibration) and 1460–1480 cm^{-1} (CH_2 wagging vibration) that are characteristics of linear polyethylene. Moreover, the terminal vinyl group gives rise to additional bands at 1642 cm^{-1} for the C=C stretching mode, 994 cm^{-1} for the in-phase plane vibration and 912 cm^{-1} for the out-of-phase plane vibration [54–56]. These FT-IR spectra once again prove the correctness of the structure of the polymerization products revealed by NMR.

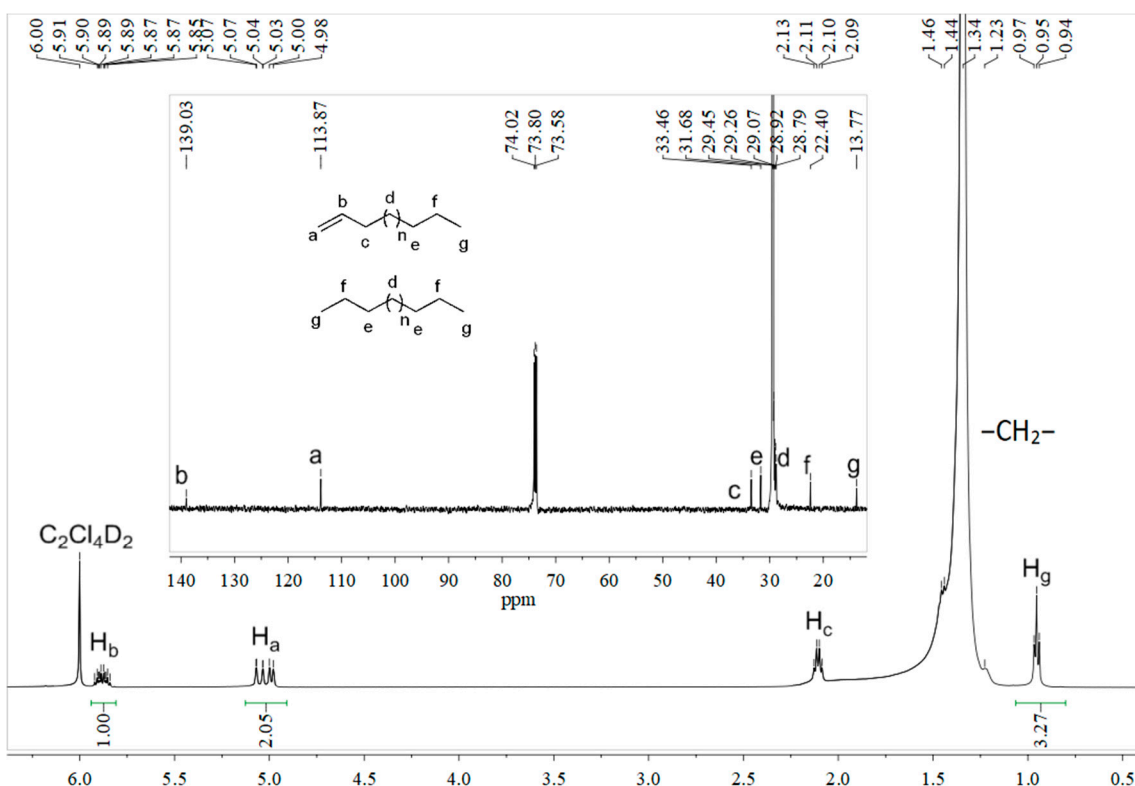


Figure 8. ^1H NMR spectrum of the polyethylene produced using **Co2**/MAO at 50 °C (entry 2, Table 3) along with an inset of the ^{13}C NMR spectrum; both spectra recorded at 100 °C in 1,1,2,2-tetrachloroethane- d_2 .

3. Experimental Section

3.1. General Considerations

Using glovebox or standard Schlenk techniques to manipulate air- or water-sensitive materials in a nitrogen atmosphere, toluene was refluxed over sodium for 48 h and then distilled under a nitrogen atmosphere prior to use. Ethylene was purchased from Beijing Yansan Petrochemical Corp (Beijing, China). Methylaluminoxane (MAO, 1.46 M solution in toluene) and modified methylaluminoxane (MMAO, 1.93 M solution in *n*-heptane) were purchased from Akzo Nobel Corp. Other reagents were purchased from Acros or local suppliers. Additionally, FT-IR spectra and elemental analyses were tested, respectively, on a PerkinElmer System 2000 FT-IR spectrometer (Perkin-Elmer, Waltham, MA, USA) and a Flash EA 1112 microanalyzer (Thermo Fisher Scientific, Waltham, MA, USA). M_w (molecular weight) and M_w/M_n (molecular weight distribution) of the resultant polyethylene were determined by Agilent PLGPC 220 at 150 °C using 1,2,4-trichlorobenzene as the solvent (PL Corp., England). While DSC traces and melting temperatures (T_m) of these polyethylenes were obtained from the second scanning run on a PerkinElmer TA-Q2000 DSC analyzer (Perkin-Elmer, Waltham, MA, USA). High temperature ^1H and ^{13}C NMR spectra of the polyethylene were recorded on a Bruker AVANCE III 500 MHz (Bruker, Fällanden, Switzerland) at 100 °C, with a spectral frequency of 499.92 MHz and 125.70 MHz, respectively. The test samples were prepared by dissolving 40 mg polyethylene in 1,1,2,2-tetrachloroethane- d_2 (2 mL) with a heat gun. Operating conditions were as follows: acquisition time (0.50 s for ^{13}C NMR and 2.18 s for ^1H NMR), relaxation delay (5.0 s for ^{13}C NMR and 2.0 s for ^1H NMR), spectral width (32.8947 kHz for ^{13}C NMR and 15.0000 kHz for ^1H NMR), number of scans (1578 for ^{13}C NMR and 256 for ^1H NMR). 2-benzoyl-5,6,7-trihydroquinolin-8-one, 2,4-dibenzhydryl-6-methylaniline (**A1**), 4-benzhydryl-2,6-dimethylaniline (**A2**), 2-benzhydryl-4,6-dimethylaniline (**A3**), 2,4-dibenzhydryl-6-ethylaniline (**A4**), 2,4-dibenzhydryl-6-isopropylaniline (**A5**) and 2,4-dibenzhydryl-6-fluoroaniline (**A6**), were prepared followed the synthesis procedures based on related literature procedures [57–59].

3.2. Synthesis of [2-(ArN=CPh)-8-(NAr)-C₉H₈N]CoCl₂ (**Co1–Co6**)

The cobalt complexes **Co1–Co6** were prepared by the one-pot reaction of 2-benzoyl-5,6,7-trihydroquinolin-8-one, corresponding anilines and CoCl₂·6H₂O in acetic acid. A general synthetic procedure for **Co1** was as follows: a suspension of 2-benzoyl-5,6,7-trihydroquinolin-8-one (0.063 g, 0.25 mmol) and 2,4-dibenzhydryl-6-methylaniline (**A1**) (0.43 g, 1.0 mmol) with CoCl₂·6H₂O (0.048 g, 0.20 mmol) in acetic acid (10 mL) was refluxed for 6 h. After cooling to room temperature, the reaction mixture was concentrated and removed the majority of the solvent by using rotary evaporator. Then, a mixture of diethyl ether (8 mL) and dichloromethane (2 mL) was added to completely dissolve the residue. Hexane (25 mL) was then added to precipitate the product. After filtration, the solid was washed with a mixture of hexane and diethyl ether (3 × 15 mL; v:v = 5:1) and dried under reduced pressure to give a yellow powder **Co1** (0.13 g, 43%). FT-IR (cm^{−1}): 3665(w), 2970(m), 1598(ν_{C=N}, m), 1559(s), 1531(s), 1475(m), 1449(s), 1266(m), 1075(m), 1033(m), 744(m), 700(s). Anal. Calcd for C₈₂H₆₇Cl₂CoN₃ (1224.29): H, 5.52; N, 3.43; C, 80.45. Found: H, 5.30; N, 3.25; C, 80.52%.

Characterization data for **Co2** (yellow powder, 0.13 g, 57%): FT-IR (cm^{−1}): 3669(w), 3054(w), 2967(m), 1604(ν_{C=N}, s), 1563(s), 1500(s), 1447(m), 1268(w), 1225(s), 1158(m), 1034(m), 833(m), 699(s). Anal. Calcd for C₅₈H₅₁Cl₂CoN₃ (919.90): H, 5.59; N, 4.57; C, 75.73. Found: H, 5.59; N, 4.47; C, 75.43%.

Characterization data for **Co3** (yellow powder, 0.10 g, 45%): FT-IR (cm^{−1}): 3664(w), 2969(m), 2157(w), 2025(w), 1972(w), 1599(ν_{C=N}, m), 1505(s), 1447(m), 1266(m), 1225(s), 1159(m), 1075(m), 1036(m), 840(s), 699(s). Anal. Calcd for C₅₈H₅₁Cl₂CoN₃ (919.90): H, 5.59; N, 4.57; C, 75.73. Found: H, 5.39; N, 4.36; C, 75.75%.

Characterization data for **Co4** (yellow powder, 0.21 g, 60%): FT-IR (cm^{−1}): 3057(w), 3025(w), 2361(m), 1596(ν_{C=N}, m), 1494(s), 1447(s), 1266(m), 1031(m), 744(s), 699(s). Anal.

Calcd for $C_{84}H_{71}Cl_2CoN_3$ (1252.35): H, 5.71; N, 3.36; C, 80.56. Found: H, 5.52; N, 3.25; C, 80.71%.

Characterization data for **Co5** (yellow powder, 0.19 g, 53%): FT-IR (cm^{-1}): 3669(w), 2967(m), 1599($\nu_{\text{C}=\text{N}}$, m), 1499(s), 1447(s), 1266(m), 1224(m), 1077(m), 1037(m), 829(m), 742(m), 699(s). Anal. Calcd for $C_{86}H_{75}Cl_2CoN_3$ (1280.40): H, 5.90; N, 3.28; C, 80.67. Found: H, 5.89; N, 3.29; C, 80.77%.

Characterization data for **Co6** (yellow powder, 0.20 g, 65%): FT-IR (cm^{-1}): 3667(w), 2969(m), 1600($\nu_{\text{C}=\text{N}}$, m), 1557(s), 1527(m), 1472(s), 1450(s), 1425(m), 1268(m), 1031(m), 745(m), 700(s). Anal. Calcd for $C_{80}H_{61}Cl_2CoF_2N_3$ (1232.22): H, 4.99; N, 3.41; C, 77.98. Found: H, 4.89; N, 3.32; C, 78.19%.

3.3. X-ray Crystallographic Studies

The single crystals of **Co2** and **Co5** suitable for X-ray diffraction analysis were grown at room temperature by the layering of hexane onto the solution of the corresponding cobalt complex in which the solvent was the mixture of dichloromethane and diethyl ether. Data collection for **Co2** and **Co5** was carried out on XtaLAB Synergy-R single-crystal diffractometer (Rigaku Corp., Japan) with mirror-monochromatic Cu-K α radiation ($\lambda = 1.54184 \text{ \AA}$). During data collection, the crystal was kept at a steady temperature ($T = 169.99(13) \text{ K}$). The structure was solved with SHELXT (Sheldrick, Göttingen, Germany, 2015) [60] solution program by using Olex2 as the graphical interface. The model was refined with SHELXL (Sheldrick, Göttingen, Germany, 2015) [61] using full matrix least squares on F^2 . The free solvent molecules were removed by using the SQUEEZE option of the PLATON software (Spek, Utrecht, The Netherlands, 2008) [62]. Details of the X-ray structure determinations and refinements are provided in Table S1.

3.4. Procedures for Ethylene Polymerization

3.4.1. Ethylene Polymerization under 1 atm Ethylene

Using freshly distilled toluene (30 mL) to dissolve cobalt pre-catalyst (2.0 μmol) in a Schlenk tube. Polymerization temperature was finely controlled by keeping the reactor in water bath. Then the required amount of co-catalyst (MAO or MMAO) was added by syringe and the reaction mixture was stirred under 1 atm ethylene pressure. After the required polymerization time (30 min), the vessel was evacuated, and the mixture was quenched with 10% HCl solution in ethanol. Finally, the precipitated polymer was filtered, washed with ethanol, and dried under vacuum at 50 °C for 24 h and weighed.

3.4.2. Ethylene Polymerization under 5 or 10 atm Ethylene

The higher-pressure ethylene polymerization was conducted in a stainless-steel autoclave (250 mL capacity), which was equipped with a mechanical stirrer, a temperature probe, and an ethylene pressure control system. Firstly, the stainless-steel autoclave was evacuated and backfilled by nitrogen or ethylene for three times. When the stainless-steel autoclave was cooled to desired polymerization temperature, under ethylene atmosphere, freshly distilled toluene (100 mL), co-catalysts (MAO or MMAO), and the toluene solution with cobalt pre-catalyst (2.0 μmol) were injected successively into the autoclave using syringes. Then, the autoclave was immediately pressurized to the desired pressure and this pressure level was maintained for the required reaction time. After the desired reaction time, stop the mechanical stirrer, cool the autoclave using ice-water bath and vent the excess ethylene. The reaction mixture was quenched with 10% HCl solution in ethanol. Finally, the precipitated polymer was filtered, washed with ethanol, and dried under vacuum at 50 °C for 24 h and weighed.

4. Conclusions

A series of cobalt dichloride complexes ligated by 2-(arylimino)benzylidene-8- arylimino-5,6,7-trihydroquinoline has been synthesized and fully characterized. On activation with either MAO or MMAO, all pre-catalysts **Co1–Co6** showed high activities toward ethylene

polymerization, while **Co**/MAO system usually had more effective catalytic behavior. In particular, 2,6-dimethyl-substituted **Co2** with the smallest steric hindrance displayed the highest activity up to 16.5×10^6 g (PE) mol $^{-1}$ (Co) h $^{-1}$ among this set at 50 °C. Moreover, *ortho*-fluoro substituted **Co6** was the second most active pre-catalyst due to its strong electron-withdrawing properties. In terms of thermostability of catalysts, **Co6**/MAO system still revealed appreciable activity (2.9×10^6 g (PE) mol $^{-1}$ (Co) h $^{-1}$) even at 70 °C, which may be due to the introduction of a fused alkyl ring and an imino C-phenyl group. Compared with cobalt complexes with 4,4'-difluorobenzhydryl and other cobalt analogues, these cobalt pre-catalysts in the current work could produce polyethylene with narrower molecular weight dispersities (1.3–3.1), indicating the positive influence of benzhydryl substitution on the single site catalytic behavior of cobalt catalysts. According to the end-group analysis results of the resultant polyethylene, polymers with vinyl end groups ($-\text{CH}=\text{CH}_2$) were confirmed as the main product, indicating β -H elimination was the major chain termination pathway. On controlling the reaction parameters, different molecular weights (1.7–386.6 kg mol $^{-1}$) of polyethylene with narrow PDIs (1.3–3.1) will be obtained. Therefore, we believe this kind of cobalt pre-catalysts has the potential to produce lubricants and colorants for industrial plastics processing in the future [41].

Supplementary Materials: The following supporting information can be downloaded at: <https://www.mdpi.com/article/10.3390/catal12101119/s1>, Table S1: Crystal data and structure refinements for **Co2** and **Co5**, Figure S1: For **Co6**/MMAO: (a) GPC traces of the polyethylene obtained at different run temperatures and (b) plots of catalytic activity and M_w of the resultant PE as a function of reaction temperature (entries 1–4, Table 4), Figure S2: For **Co6**/MMAO: (a) GPC traces of the polymers obtained at different Al:Co molar ratios and (b) plots of catalytic activity and M_w of the resultant PE as a function of Al:Co molar ratio (entries 2, 5–8, Table 4), Figure S3: For **Co6**/MMAO: (a) GPC traces of the polyethylene obtained over the course of time and (b) plots of catalytic activity and M_w of the resultant PE as a function of reaction time (entries 5, 9–12, Table 4), Figure S4: Catalytic activities and molecular weight of the polyethylenes produced by **Co1**–**Co6**; MMAO as co-catalyst in each case (entries 1–6, Table 5), Figure S5: ^1H NMR spectrum of the polyethylene obtained using **Co2**/MMAO at 40 °C (entry 2, Table 5) along with an inset of the ^{13}C NMR spectrum; both spectra recorded at 100 °C in 1,1,2,2-tetrachloroethane- d_2 , Figure S6: DEPT-135 ^{13}C NMR spectrum of the polyethylene obtained using **Co2**/MAO at 50 °C (entry 2, Table 3), Figure S7: DEPT-135 ^{13}C NMR spectrum of the polyethylene obtained using **Co2**/MMAO at 40 °C (entry 2, Table 5), Figure S8: FT-IR spectra of the polyethylene samples generated using **Co2**/MAO (top, entry 2, Table 3) and **Co6**/MAO (middle, entry 2, Table 2 and bottom, entry 8, Table 2), Figure S9: FT-IR spectra of the polyethylene generated using **Co2**/MMAO (top, entry 2, Table 5) and **Co6**/MMAO (middle, entry 5, Table 4 and bottom, entry 7, Table 4).

Author Contributions: Conceptualization, W.-H.S.; formal analysis, Z.Z.; investigation, Z.Z.; data curation, Z.Z.; writing—original draft preparation, Z.Z.; writing—review and editing, Z.Z., Q.Z., Y.M. and W.-H.S.; visualization, Z.Z., M.H., M.L. and Y.S.; supervision, W.-H.S.; project administration, W.-H.S.; funding acquisition, W.-H.S. All authors have read and agreed to the published version of the manuscript.

Funding: This work is supported by the National Natural Science Foundation of China (21871275).

Data Availability Statement: CCDC 2160864 and CCDC 2160865 contain the supplementary crystallographic data for complex **Co2** and **Co5**, respectively.

Conflicts of Interest: The authors declare no conflict of interest.

References

1. Gibson, V.C.; Redshaw, C.; Solan, G.A. Bis(imino)pyridines: Surprisingly reactive ligands and a gateway to new families of catalysts. *Chem. Rev.* **2007**, *107*, 1745–1776. [[CrossRef](#)] [[PubMed](#)]
2. Bianchini, C.; Giambastiani, G.; Luconi, L.; Meli, A. Olefin oligomerization, homopolymerization and copolymerization by late transition metals supported by (imino)pyridine ligands. *Coord. Chem. Rev.* **2010**, *254*, 431–455. [[CrossRef](#)]
3. Small, B.L. Discovery and development of pyridine-bis(imine) and related catalysts for olefin polymerization and oligomerization. *Acc. Chem. Res.* **2015**, *48*, 2599–2611. [[CrossRef](#)] [[PubMed](#)]

4. Ma, Z.; Yang, W.; Sun, W.-H. Recent progress on transition metal (Fe, Co, Ni, Ti and V) complex catalysts in olefin polymerization with high thermal stability. *Chin. J. Chem.* **2017**, *35*, 531–540. [[CrossRef](#)]
5. Wang, Z.; Solan, G.A.; Zhang, W.; Sun, W.-H. Carbocyclic-fused N,N,N-pincer ligands as ring-strain adjustable supports for iron and cobalt catalysts in ethylene oligo-/polymerization. *Coord. Chem. Rev.* **2018**, *363*, 92–108. [[CrossRef](#)]
6. Bariashir, C.; Jiang, S.; Ma, Y.; Solan, G.A.; Sun, Y.; Sun, W.-H. Recent advances in homogeneous chromium catalyst design for ethylene tri-, tetra-, oligo- and polymerization. *Coord. Chem. Rev.* **2019**, *385*, 208–229. [[CrossRef](#)]
7. Small, B.L.; Brookhart, M. Iron-based catalysts with exceptionally high activities and selectivities for oligomerization of ethylene to linear α -Olefins. *J. Am. Chem. Soc.* **1998**, *120*, 7143–7144. [[CrossRef](#)]
8. Liu, M.; Brookhart, M. CF₃O-Functionalized bis(arylimino)pyridine cobalt ethylene polymerization catalysts: Harnessing solvent effects on performance and polymer properties. *Organometallics* **2022**. [[CrossRef](#)]
9. Liu, T.; Liu, M.; Ma, Y.; Solan, G.A.; Liang, T.; Sun, W.-H. Cobalt catalysts bearing ortho-(4,4'-dichlorobenzhydryl) substituents and their use in generating narrowly dispersed polyethylene of high linearity. *Eur. J. Inorg. Chem.* **2022**, e202200396. [[CrossRef](#)]
10. Bianchini, C.; Giambastiani, G.; Rios, I.G.; Mantovani, G.; Meli, A.; Segarra, A.M. Ethylene oligomerization, homopolymerization and copolymerization by iron and cobalt catalysts with 2,6-(bis-organylimino)pyridyl ligands. *Coord. Chem. Rev.* **2006**, *250*, 1391–1418. [[CrossRef](#)]
11. Flisak, Z.; Sun, W.-H. Progression of diiminopyridines: From single application to catalytic versatility. *ACS. Catal.* **2015**, *5*, 4713–4724. [[CrossRef](#)]
12. Ma, J.; Feng, C.; Wang, S.; Zhao, K.-Q.; Sun, W.-H.; Redshaw, C.; Solan, G.A. Bi- and tridentate imino-based iron and cobalt pre-catalysts for ethylene oligo-/polymerization. *Inorg. Chem. Front.* **2014**, *1*, 14–34. [[CrossRef](#)]
13. Gao, R.; Sun, W.-H.; Redshaw, C. Nickel complex pre-catalysts in ethylene polymerization: New approaches to elastomeric materials. *Catal. Sci. Technol.* **2013**, *3*, 1172–1179. [[CrossRef](#)]
14. Zhang, W.; Sun, W.-H.; Redshaw, C. Tailoring iron complexes for ethylene oligomerization and/or polymerization. *Dalton. Trans.* **2013**, *42*, 8988–8997. [[CrossRef](#)]
15. Jie, S.; Sun, W.-H.; Xiao, T. Prospects and crucial problems in oligomerization and polymerization with iron and cobalt complex catalysts. *Chin. J. Polym. Sci.* **2010**, *28*, 299–304. [[CrossRef](#)]
16. Xiao, T.; Zhang, W.; Lai, J.; Sun, W.-H. Iron-oriented ethylene oligomerization and polymerization: The iron age or a flash in the pan. *Comptes Rendus Chim.* **2011**, *14*, 851–855. [[CrossRef](#)]
17. Sun, W.-H.; Zhang, S.; Zuo, W. Our variations on iron and cobalt catalysts toward ethylene oligomerization and polymerization. *Comptes Rendus Chim.* **2008**, *11*, 307–316. [[CrossRef](#)]
18. Sun, W.-H.; Zhao, W.; Yu, J.; Zhang, W.; Hao, X.; Redshaw, C. Enhancing the activity and thermal stability of iron precatalysts using 2-(1-[2,6-bis[bis(4-fluorophenyl)methyl]-4-methylphenylimino]ethyl)-6-[1-(arylimino)ethyl]pyridines. *Macromol. Chem. Phys.* **2012**, *213*, 1266–1273. [[CrossRef](#)]
19. Xing, Q.; Zhao, T.; Du, S.; Yang, W.; Liang, T.; Redshaw, C.; Sun, W.-H. Biphenyl-bridged 6-(1-aryliminoethyl)-2-iminopyridyl cobalt complexes: Synthesis, characterization, and ethylene polymerization behavior. *Organometallics* **2014**, *33*, 1382–1388. [[CrossRef](#)]
20. Cao, X.; He, F.; Zhao, W.; Cai, Z.; Hao, X.; Shiono, T.; Redshawd, C.; Sun, W.-H. 2-[1-(2,6-dibenzhydryl-4-chlorophenylimino)ethyl]-6-[1-(arylimino)ethyl]pyridyliron(II) dichlorides: Synthesis, characterization and ethylene polymerization behavior. *Polymer* **2012**, *53*, 1870–1880. [[CrossRef](#)]
21. Wang, S.; Li, B.; Liang, T.; Redshaw, C.; Li, Y.; Sun, W.-H. Synthesis, characterization and catalytic behavior toward ethylene of 2-[1-(4,6-dimethyl-2-benzhydrylphenylimino)ethyl]-6-[1-(arylimino)ethyl]pyridylmetal (iron or cobalt) chlorides. *Dalton. Trans.* **2013**, *42*, 9188–9197. [[CrossRef](#)] [[PubMed](#)]
22. Yu, J.; Liu, H.; Zhang, W.; Hao, X.; Sun, W.-H. Access to highly active and thermally stable iron procatalysts using bulky 2-[1-(2,6-dibenzhydryl-4-methylphenylimino)ethyl]-6-[1-(arylimino)ethyl]pyridine ligands. *Chem. Commun.* **2011**, *47*, 3257–3259. [[CrossRef](#)] [[PubMed](#)]
23. Small, B.L.; Brookhart, M.; Bennett, A.M.A. Highly active iron and cobalt catalysts for the polymerization of ethylene. *J. Am. Chem. Soc.* **1998**, *120*, 4049–4050. [[CrossRef](#)]
24. Britovsek, G.J.P.; Gibson, V.C.; Kimberley, B.S.; Maddox, P.J.; McTavish, S.J.; Solan, G.A.; White, A.J.P.; Williams, D.J. Novel olefin polymerization catalysts based on iron and cobalt. *Chem. Commun.* **1998**, 849–850. [[CrossRef](#)]
25. Britovsek, G.J.P.; Bruce, M.; Gibson, V.C.; Kimberley, B.S.; Maddox, P.J.; Mastroianni, S.; McTavish, S.J.; Redshaw, C.; Solan, G.A.; Stromberg, S.; et al. Iron and cobalt ethylene polymerization catalysts bearing 2,6-bis(imino)pyridyl ligands: Synthesis, structures, and polymerization studies. *J. Am. Chem. Soc.* **1999**, *121*, 8728–8740. [[CrossRef](#)]
26. Britovsek, G.J.P.; Mastroianni, S.; Solan, G.A.; Baugh, S.P.D.; Redshaw, C.; Gibson, V.C.; White, A.J.P.; Williams, D.J.; Elsegood, M.R.J. Oligomerisation of ethylene by bis(imino)pyridyliron and -cobalt complexes. *Chem. Eur. J.* **2000**, *6*, 2221–2231. [[CrossRef](#)]
27. Knijnenburg, Q.; Gambarotta, S.; Budzelaar, P.H.M. Ligand-centred reactivity in diiminepyridine complexes. *Dalton. Trans.* **2006**, 5442–5448. [[CrossRef](#)]
28. Scott, J.; Gambarotta, S.; Korobkov, I.; Budzelaar, P.H.M. Metal versus ligand alkylation in the reactivity of the (bis-iminopyridinato) Fe catalyst. *J. Am. Chem. Soc.* **2005**, *127*, 13019–13029. [[CrossRef](#)]
29. Sugiyama, H.; Aharonian, G.; Gambarotta, S.; Yap, G.P.A.; Budzelaar, P.H.M. Participation of the α,α' -diiminopyridine ligand system in reduction of the metal center during alkylation. *J. Am. Chem. Soc.* **2002**, *124*, 12268–12274. [[CrossRef](#)]

30. Bouwkamp, M.W.; Lobkovsky, E.; Chirik, P.J. Bis(imino)pyridine ligand deprotonation promoted by a transient iron amide. *Inorg. Chem.* **2006**, *45*, 2–4. [[CrossRef](#)]
31. Smit, T.M.; Tomov, A.K.; Britovsek, G.J.P.; Gibson, V.C.; White, A.J.P.; Williams, D.J. The effect of imine-carbon substituents in bis(imino)pyridine-based ethylene polymerisation catalysts across the transition series. *Catal. Sci. Technol.* **2012**, *2*, 643–655. [[CrossRef](#)]
32. McTavish, S.; Britovsek, G.J.P.; Smit, T.M.; Gibson, V.C.; White, A.J.P.; Williams, D.J. Iron-based ethylene polymerization catalysts supported by bis(imino)pyridine ligands: Derivatization via deprotonation/alkylation at the ketimine methyl position. *J. Mol. Catal. A-Chem.* **2007**, *261*, 293–300. [[CrossRef](#)]
33. Sun, W.-H.; Kong, S.; Chai, W.; Shiono, T.; Redshaw, C.; Hu, X.; Guo, C.; Hao, X. 2-(1-(Arylimino)ethyl)-8-arylimino-5,6,7-trihydroquinolylcobalt dichloride: Synthesis and polyethylene wax formation. *Appl. Catal. A-Gen.* **2012**, *447–448*, 67–73. [[CrossRef](#)]
34. Huang, F.; Zhang, W.; Yue, E.; Liang, T.; Hu, X.; Sun, W.-H. Controlling the molecular weights of polyethylene waxes using the highly active precatalysts of 2-(1-aryliminoethyl)-9-arylimino-5,6,7,8-tetrahydrocycloheptapyridylcobalt chlorides: Synthesis, characterization, and catalytic behavior. *Dalton Trans.* **2016**, *45*, 657–666. [[CrossRef](#)] [[PubMed](#)]
35. Ba, J.; Du, S.; Yue, E.; Hu, X.; Flisak, Z.; Sun, W.-H. Constrained formation of 2-(1-(arylimino)ethyl)-7-arylimino-6,6-dimethyl cyclopentapyridines and their cobalt(II) chloride complexes: Synthesis, characterization and ethylene polymerization. *RSC. Adv.* **2015**, *5*, 32720–32729. [[CrossRef](#)]
36. Huang, F.; Zhang, W.; Sun, Y.; Hu, X.; Solan, G.A.; Sun, W.-H. Bis(imino)-6,7-dihydro-5H-quinoline-cobalt complexes as highly active catalysts for the formation of vinyl-terminated PE waxes; steps towards inhibiting deactivation pathways through targeted ligand design. *New. J. Chem.* **2016**, *40*, 8012–8023. [[CrossRef](#)]
37. Han, M.; Zuo, Z.; Ma, Y.; Solan, G.A.; Hu, X.; Liang, T.; Sun, W.-H. Thermally stable and highly active cobalt precatalysts for vinyl-polyethylenes with narrow polydispersities: Integrating fused-ring and imino-carbon protection into ligand design. *RSC. Adv.* **2021**, *11*, 39869–39878. [[CrossRef](#)]
38. Zuo, Z.; Han, M.; Ma, Y.; Solan, G.A.; Hu, X.; Liang, T.; Sun, W.-H. Fluorinated bis(arylimino)-6,7-dihydro-5H-quinoline-cobalt polymerization catalysts: Electronic versus steric modulation in the formation of vinyl-terminated linear PE waxes. *Appl. Organomet. Chem.* **2022**, *36*, e6500. [[CrossRef](#)]
39. Du, S.; Zhang, W.; Yue, E.; Huang, F.; Liang, T.; Sun, W.-H. α,α' -Bis(arylimino)-2,3:5,6-bis(pentamethylene)pyridylcobalt chlorides: Synthesis, characterization, and ethylene polymerization behavior. *Eur. J. Inorg. Chem.* **2016**, *11*, 1748–1755. [[CrossRef](#)]
40. Wang, Z.; Ma, Y.; Guo, J.; Liu, Q.; Solan, G.A.; Liang, T.; Sun, W.-H. Bis(imino)pyridines fused with 6- and 7-membered carbocyclic rings as *N,N,N*-scaffolds for cobalt ethylene polymerization catalysts. *Dalton Trans.* **2019**, *48*, 2582–2591. [[CrossRef](#)]
41. Wang, K.; Wedeking, K.; Zuo, W.; Zhang, D.; Sun, W.-H. Iron(II) and cobalt(II) complexes bearing N-((pyridin-2-yl)methylene)quinolin-8-amine derivatives: Synthesis and application to ethylene oligomerization. *J. Organomet. Chem.* **2008**, *693*, 1073–1080. [[CrossRef](#)]
42. Zhang, W.; Wang, S.; Du, S.; Guo, C.-Y.; Hao, X.; Sun, W.-H. 2-(1-(2,4-Bis((di(4-fluorophenyl)methyl)-6-methylphenylimino)ethyl)-6-(1-(arylimino)ethyl)pyridylmetal (iron or cobalt) complexes: Synthesis, characterization, and ethylene polymerization behavior. *Macromol. Chem. Phys.* **2014**, *215*, 1797–1809. [[CrossRef](#)]
43. Zhao, W.; Yu, J.; Song, S.; Yang, W.; Liu, H.; Hao, X.; Redshaw, C.; Sun, W.-H. Controlling the ethylene polymerization parameters in iron pre-catalysts of the type 2-[1-(2,4-dibenzhydryl-6-methylphenylimino)ethyl]-6-[1-(arylimino)ethyl] pyridyliron dichloride. *Polymer* **2012**, *53*, 130–137. [[CrossRef](#)]
44. Lai, J.; Zhao, W.; Yang, W.; Redshaw, C.; Liang, T.; Liu, Y.; Sun, W.-H. 2-[1-(2,4-dibenzhydryl-6-methylphenylimino)ethyl]-6-[1-(arylimino)ethyl] pyridylcobalt(II) dichlorides: Synthesis, characterization and ethylene polymerization behavior. *Polym. Chem.* **2012**, *3*, 787–793. [[CrossRef](#)]
45. Guo, L.; Zada, M.; Zhang, W.; Vignesh, A.; Zhu, D.; Ma, Y.; Liang, T.; Sun, W.-H. Highly linear polyethylenes tailored with 2,6-bis[1-(*p*-dibenzo-cycloheptylarylimino)ethyl]-pyridylcobalt dichlorides. *Dalton Trans.* **2019**, *48*, 5604–5613. [[CrossRef](#)]
46. Zhang, R.; Han, M.; Oleynik, I.V.; Solan, G.A.; Oleynik, I.I.; Ma, Y.; Liang, T.; Sun, W.-H. Boosting activity, thermostability, and lifetime of iron ethylene polymerization catalysts through gem-dimethyl substitution and incorporation of ortho-cycloalkyl substituents. *Appl. Organomet. Chem.* **2021**, *35*, e6376. [[CrossRef](#)]
47. Zhang, M.; Gao, R.; Hao, X.; Sun, W.-H. 2-Oxazoline/benzoxazole-1,10-phenanthrolinylmetal (iron, cobalt or nickel) dichloride: Synthesis, characterization and their catalytic reactivity for the ethylene oligomerization. *J. Organomet. Chem.* **2008**, *693*, 3867–3877. [[CrossRef](#)]
48. Kulkarni, N.V.; Elkin, T.; Tumaniskii, B.; Botoshansky, M.; Shimon, L.J.; Eisen, M.S. Asymmetric Bis(formamidinate) Group 4 Complexes: Synthesis, Structure and Their Reactivity in the Polymerization of α -Olefins. *Organometallics* **2014**, *33*, 3119–3136. [[CrossRef](#)]
49. Elkin, T.; Kulkarni, N.V.; Tumaniskii, B.; Botoshansky, M.; Shimon, L.J.; Eisen, M.S. Synthesis and structure of Group 4 symmetric amidinate complexes and their reactivity in the polymerization of α -olefins. *Organometallics* **2013**, *32*, 6337–6352. [[CrossRef](#)]
50. Zhang, Y.; Suo, H.; Huang, F.; Liang, T.; Hu, X.; Sun, W.-H. Thermo-sTable 2-(arylimino)benzylidene-9-arylimino-5,6,7,8-tetrahydrocyclohepta[b]pyridyliron(II) precatalysts toward ethylene polymerization and highly linear polyethylenes. *J. Polym. Sci. Pol. Chem.* **2016**, *55*, 830–842. [[CrossRef](#)]

51. Zhang, Q.; Wu, N.; Xiang, J.; Solan, G.A.; Suo, H.; Ma, Y.; Liang, T.; Sun, W.-H. Bis-cycloheptyl-fused bis(imino)pyridine-cobalt catalysts for PE wax formation: Positive effects of fluoride substitution on catalytic performance and thermal stability. *Dalton Trans.* **2020**, *49*, 9425–9437. [[CrossRef](#)] [[PubMed](#)]
52. Han, M.; Oleynik, I.I.; Liu, M.; Ma, Y.; Oleynik, I.V.; Solan, G.A.; Liang, T.; Sun, W.-H. Ring size enlargement in an *ortho*-cycloalkyl-substituted bis(imino)pyridine-cobalt ethylene polymerization catalyst and its impact on performance and polymer properties. *Appl. Organomet. Chem.* **2022**, *36*, e6529. [[CrossRef](#)]
53. Guo, L.; Zhang, W.; Cao, F.; Jiang, Y.; Zhang, R.; Ma, Y.; Solan, G.A.; Sun, Y.; Sun, W.-H. Remote dibenzocycloheptyl substitution on a bis(arylimino)pyridyl-iron ethylene polymerization catalyst; enhanced thermal stability and unexpected effects on polymer properties. *Polym. Chem.* **2021**, *12*, 4214–4225. [[CrossRef](#)]
54. Martinez-Romo, A.; Gonzalez-Mota, R.; Soto-Bernal, J.J.; Rosales-Candelas, I. Investigating the degradability of HDPE, LDPE, PE-BIO, and PE-OXO films under UV-B radiation. *J. Spectrosc.* **2015**, *2015*, 586514. [[CrossRef](#)]
55. Glenz, W.; Peterlin, A. IR-studies of drawn polyethylene part III. The orientation of vinyl and methyl end-groups. *Makromol. Chem.* **1971**, *150*, 163–177. [[CrossRef](#)]
56. Jung, M.R.; Horgen, F.D.; Orski, S.V.; Rodriguez, V.; Beers, C.K.L.; Balazs, G.H.; Jones, T.T.; Work, T.M.; Brignac, K.C.; Royer, S.-J.; et al. Validation of ATR FT-IR to identify polymers of plastic marine debris, including those ingested by marine organisms. *Mar. Pollut. Bull.* **2018**, *127*, 704–716. [[CrossRef](#)] [[PubMed](#)]
57. Shaw, P.; Kennedy, A.R.; Nelson, D.J. Synthesis and characterisation of an *N*-heterocyclic carbene with spatially-defined steric impact. *Dalton Trans.* **2016**, *45*, 11772–11780. [[CrossRef](#)]
58. Guo, J.; Zhang, W.; Oleynik, I.I.; Solan, G.A.; Oleynik, I.V.; Liang, T.; Sun, W.-H. Probing the effect of *ortho*-cycloalkyl ring size on activity and thermostability in cycloheptyl-fused *N,N,N*-iron ethylene polymerization catalysts. *Dalton Trans.* **2020**, *49*, 136–146. [[CrossRef](#)]
59. Huang, F.; Xing, Q.; Liang, T.; Flisak, Z.; Ye, B.; Hu, X.; Yang, W.; Sun, W.-H. 2-(1-aryliminoethyl)-9-arylimino-5,6,7,8-tetrahydro-cycloheptapyridyl iron(II) dichloride: Synthesis, characterization, and the highly active and tunable active species in ethylene polymerization. *Dalton Trans.* **2014**, *43*, 16818–16829. [[CrossRef](#)]
60. Sheldrick, G.M. *SHELXT*—Integrated space-group and crystal- structure determination. *Acta. Cryst.* **2015**, *A71*, 3–8. [[CrossRef](#)]
61. Sheldrick, G.M. Crystal structure refinement with *SHELXL*. *Acta. Cryst.* **2015**, *C71*, 3–8.
62. Spek, L. Bis-cycloheptyl-fused bis(imino)pyridine-cobalt catalysts for PE wax formation: Positive effects of fluoride substitution on catalytic performance and thermal stability. *Acta. Cryst. D-Biol. Cryst.* **2009**, *65*, 148–155. [[CrossRef](#)] [[PubMed](#)]